Effect of corrosion on the soil-structure interaction of CSP culverts

Alex Campbell & Hany El Naggar
Department of Civil and Resource Engineering – Dalhousie University, Halifax, Nova Scotia, Canada

GEOQuébec 2015
Challenges from North to South
Des défis du Nord au Sud

ABSTRACT
Adequate long-term performance of buried culvert structures depends in part on the durability of the steel in service. In some cases, culverts may experience degradation when exposed to chloride-contaminated groundwater. This paper presents a three-dimensional finite element model to examine the influence of corrosion on the stability of circular corrugated steel culverts. The geometrical and material details of the backfill, as well as the construction process, culvert geometry, and earth and vehicle loads were considered in the model. A new approach to account for the effects of backfill compaction is introduced. The culvert behaviour was simulated using a non-linear finite element model (FEM) that accounts for soil-structure interaction and the non-linear stress-strain response of the culvert. The non-linear FEM was used to calculate structural forces in culverts with corroded inverts and that are subjected to standard truck loads.

RÉSUMÉ
La performance adéquate à long terme des ponceaux enterrés dépend en partie de la durabilitée de l'acier en service. Dans certains cas, les ponceaux peuvent se dégrader en raison de l'eau souterraine contaminée par le chlorure. Cet article présente une modèle d'éléments finis en trois dimensions pour examiner l'influence de la corrosion sur la stabilité des ponceaux circulaires en acier ondulé. Les détails géométriques et des materiaux de remblai, ainsi que le processus de construction, la géométrie du ponceau, et les charges de terre et de véhicules, ont été considérés dans le modèle. Une nouvelle approche pour incorporer les effets du compactage du sol est introduit. Le comportement du ponceau a été simulé à l'aide d'un modèle d'éléments finis (MEF) non-linéaire qui représente l'interaction sol-structure et la réponse contrainte-déformation non-linéaire du ponceau. Le MEF a été utilisé pour calculer les forces dans les ponceaux avec des invertis corrodés et qui sont soumis à des charges de camion standard.

1 INTRODUCTION

Like many other countries around the world, Canada is facing a huge infrastructure deficit. Much of the existing infrastructure is approaching or has already surpassed its intended service life. As the infrastructure continues to age, the problem worsens, and the risk of failures increases. One of the most prominent types of such infrastructure is the corrugated steel pipe (CSP) culvert. The cost of culvert failures, as noted by Perrin and Chintan (2004), far exceeds that of replacement alone and is shared by government, private landowners and public citizens in terms of traffic delays. More importantly, failing infrastructure represents a serious risk to public safety. For these reasons, increasing focus over the past couple of decades has been on the maintenance of existing infrastructure systems rather than on new construction projects.

The use of CSP in culverts in North America and elsewhere in the world gained favour in the late 1950s, primarily due to its low initial cost and ease of installation. Many of the CSP culverts in service today were installed in the 1960s, 1970s and 1980s. Since the design lives of most of these CSP culverts range from about 30-50 years (USACE, 1998), it is not surprising that many of them are in need of serious attention. To make matters worse, effects of abrasion and corrosion – the two mechanisms primarily responsible for CSP degradation – have significantly reduced the service lives of many culverts. Figure 1 shows a small diameter (0.6 m) circular CSP culvert in Halifax with a severely corroded invert. Although many other corrosion patterns exist, the one shown here (i.e. concentrated within the wetted perimeter of the pipe) is typical of CSP culverts of all sizes.

Figure 1. Typical CSP culvert invert degradation.

Most agencies have by now realized the importance of good asset management; inspection programs are generally well established and culverts conditions are known, at least in subjective terms. However, reliable techniques to analyze the effects of CSP degradation with respect to the structural integrity of the culvert are still evolving, and almost exclusively rely on numerical modelling. Two-dimensional finite element models have been developed (El-Taher and Moore, 2008; Mai et al., 2014) to analyze the stability of deteriorated metal culverts. However, two-dimensional models are limited in their ability to capture three-dimensional loading effects and stress redistribution. Three-dimensional models of intact CSP culverts subjected to live loading (El-Sawy, 2003, and MacDonald, 2010) have been developed, but employ linear-elastic soil models which are unable to capture the non-linear response of the soil-steel system. Furthermore, these studies did not investigate corrosion effects. This paper presents a three-dimensional finite element model (FEM) to analyze the behaviour of corroded CSP culverts.

2 EFFECTS OF COMPACTION

Cut and cover techniques used to construct the majority of culverts involve placing the CSP on a bedding soil and enveloping it with backfill soil. In order to achieve adequate stiffness and strength of the backfill soil, it is placed and compacted in layers, often about 100 to 300 mm thick. The soil compaction causes lateral strains in the soil that are largely irrecoverable, and which result in increased lateral earth pressures. In the case of CSP culverts, lateral earth pressures force the culvert to contract in the horizontal dimension, with an associated expansion of the vertical diameter. The shape of the CSP culvert thus changes from circular to elliptical, and may result in the crown of the pipe being at a slightly higher elevation than it was prior to backfilling. This peaking effect is magnified when the backfill material is compacted.

In addition to increasing the magnitude of lateral earth pressures (some portion of which are dissipated during horizontal contraction of the CSP), compaction may also influence the distribution of lateral earth pressures near the culvert. Ingold (1979) presented an analytical method to predict the induced lateral earth pressures behind retaining walls based on the effective loading provided by the compaction equipment. The predicted lateral stress distribution is shown in Figure 2.

The distribution of induced vertical stress $\Delta\sigma'_v$ below a surface load decreases non-linearly with depth. According to classical earth pressure theories, at any point below the surface the induced horizontal stress, $\Delta\sigma'_h$, is proportional to the induced vertical stress and is calculated using equation 1:

$$\Delta\sigma'_h = K\,\Delta\sigma'_v \qquad [1]$$

where K is the coefficient of lateral earth pressure.

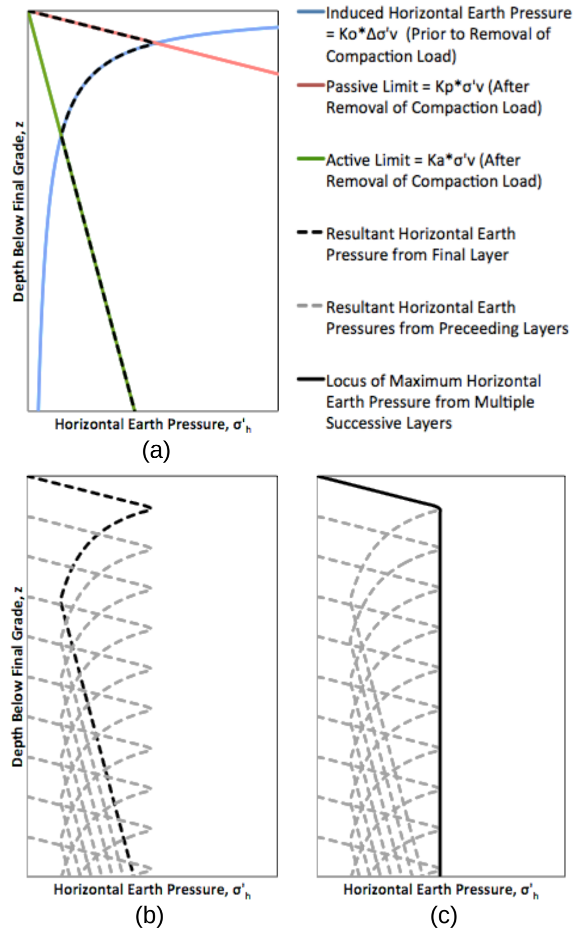

Figure 2. Development of horizontal earth pressure distribution below ground surface after compaction of multiple successive backfill layers (after Ingold (1979)).

The range of possible values of the coefficient of lateral earth pressure K is defined by the active (minimum) and passive (maximum) limits K_a and K_p, respectively. Once the effective compaction load is removed, the vertical earth pressure recovers the linear distribution it had prior to compaction. However, since the soil remains confined in the lateral direction(s), the distribution of lateral pressure retains a non-linear shape similar to that of $\Delta\sigma'_v$. Above a certain critical depth z_c, there is passive failure of the soil due to the relatively low vertical stresses near the ground surface, and the lateral pressure distribution is linear within this zone. A critical height of backfill, h_c, also exists, below which there is active failure and the distribution again becomes linear. Since backfill lift thicknesses are typically around 150 to 300 mm, this active failure does not usually occur within an individual layer. The dashed line in Figure 2(a) marks the resultant pressure distribution. As backfill layers are successively placed and compacted the lateral earth pressure envelope is approximately uniform with a magnitude defined by equation 2:

$$\Delta\sigma'_{hm} = K_p\,\gamma z_c \qquad [2]$$

3 EXPERIMENTAL MODEL

For the purpose of model calibration and evaluation, the full-scale laboratory experiments carried out by Mai et al. (2014) at Queen's University were considered.

3.1 Test Materials and Setup

As described by Mai et al. (2014), two different 1.8 m-diameter CSP specimens were exhumed from the field, then re-buried in a laboratory test pit (8 m wide, 8 m long, and 3 m deep) and subjected to surface loading. One of the specimens, designated as CSP1, had extensive corrosion along both sides of the invert, while the other specimen, designated as CSP2, was relatively intact, having only light corrosion along either side of the invert. The finite element model presented in section 4 will simulate the construction of a new (intact) culvert, and then simulate the effects of corrosion, rather than simulate the construction of an already deteriorated culvert. For this reason, only specimen CSP2 is of interest and will be discussed here. The average remaining wall thicknesses of CSP2 (Figure 3) measured using an ultrasonic thickness gauge along the west and east side of the invert (haunches) were 83 and 90%. The Young's modulus and yield strength of the steel were taken as 200 GPa and 230 MPa, respectively.

Well-graded sandy gravel (classified as GW-SW based on the USCS) was used as the backfill material. Soil compaction was achieved using a vibrating plate tamper to a compacted state of 95% Standard Proctor Density (SPD). The bedding for CSP2 consisted of a 0.6 m layer of compacted material overlain by 100 mm of loose material, while the sidefill and backfill above the crown were placed using 300 mm-thick compacted lifts.

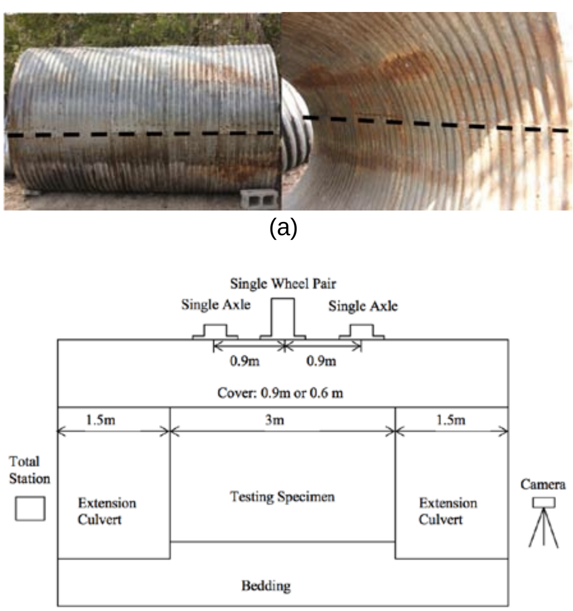

(a)

(b)

Figure 3. Specimen CSP2 and Experimental Test Setup (Mai et al. 2014)

Specimen CSP2 and the experimental test setup are shown in Figure 3. Two extension culverts measuring 1.5m in length were placed on either end of the test specimen in an effort to reduce end effects during backfilling and live loading.

3.2 Loading

Live loading was applied at the ground surface (with both 0.6 m and 0.9 m cover) via one or two hydraulically loaded steel pads to simulate loading from a single wheel (SW) pair or a single axle (SA), respectively. Each steel pad had dimensions of 250 mm by 600 mm, and a surface area of 0.15 m^2. The applied loads in each case were symmetric with respect to the transverse and longitudinal centreline of the culvert. The magnitudes of the applied loads were based on the Canadian CL-625 (Canadian Standards Association) and the AASHTO design trucks and included dynamic allowances and presence factors. The calculated design loads for 4 different scenarios are summarized in Table 1.

Table 1. Calculated Design Loads (based on (Mai et al. 2014))

Cover height, Load Type	CSA	AASHTO
0.6 m, SW[1]	112 kN	91 kN
0.6 m, SA[2]	224 kN	182 kN
0.9 m, SW	106 kN	87.5 kN
0.9 m, SA	214 kN	175 kN

[1]SW = Single Wheel Load
[2]SA = Single Axle Load

During backfilling and live loading, the change in vertical and horizontal diameters of the culverts were measured using string potentiometers at the center of the culverts, and under the load pad.

Vertical displacements along the crown and the deflected shape of the culvert at the central cross section were measured using a total station and 15 prisms attached to the inside of the culvert.

56 uniaxial strain gauges were attached to CSP2 at both the crest and valley of a corrugation in order to determine average axial strain, curvature, thrust forces and bending moments in the pipe.

4 NUMERICAL MODEL

A comprehensive three-dimensional finite element model to analyze the effects of CSP culvert corrosion was created using the commercial software Plaxis 3D.

4.1 Mesh and Boundary Conditions

The soil continuum was modelled using the ten-noded tetrahedral (3D) soil elements available in Plaxis 3D (2013). The CSP was modelled using 6-noded plate elements and the interface between the soil and CSP using 12-noded elements. A Global coarseness of "fine"

(r_e=0.7) was used with a locally refined zone around the CSP having a fineness factor of 0.5. This resulted in a mesh consisting of 41,409 elements and 71,084 nodes.

In general, the default boundary conditions were used (rollers on the sides, fixed on the bottom, and free on the top). However, temporary changes to the boundary conditions were made during the staged construction in order to capture the effects of soil compaction, as described in section 3.4.2. Although extension culverts were installed in the experimental tests, these were not included in the numerical model in order to reduce the model size. The model boundaries thus measured 8 m wide by 3 m long by 3.4 m high.

4.2 CSP Properties

Due to the additional complexity that would be introduced by explicitly modelling the corrugated geometry of the CSP, an orthotropic plain shell model was adopted as had been done by previous researchers (e.g. Moore and Taleb 1999, MacDonald 2010). Equivalent values of plate thickness, t', Elastic Modulus, E', and Shear Modulus, G', are assigned to the plate elements on the basis of equations 1 through 5. The subscripts denote the orientation of the local axis of the plate element; axis 1 is oriented in the longitudinal direction, axis 2 in the circumferential direction, and axis 3 in the direction normal (perpendicular) to the CSP plate. The conventions for material properties and structural forces with respect to the local plate axes are shown in Figure 6.

$$t' = d * \sqrt{(3/(2(1+((\pi^2 d^2)/(4b^2)))))} \quad [1]$$

$$E'_1 = (2/3)E(t/d)^3\sqrt{(2/3(1+(\pi^2 d^2)/(4b^2))^3)} \quad [2]$$

$$E'_2 = (3/2)(1+((\pi^2 d^2)/(8b^2))(Et/d)[(2/3(1+(\pi^2 d^2)/(4b^2)))^{3/2} \quad [3]$$

$$G'_{12,13} = (Gt/d) * \sqrt{(2/(3(1+(\pi^2 d^2)/(4b^2))))} \quad [4]$$

$$G'_{23} = G(t/d)^3 * (2/3)^{3/2} * (1+ (\pi^2 d^2)/(4b^2))^{5/2} \quad [5]$$

Where t is the steel plate thickness, d is the depth of corrugation, and b is half the corrugation wavelength.

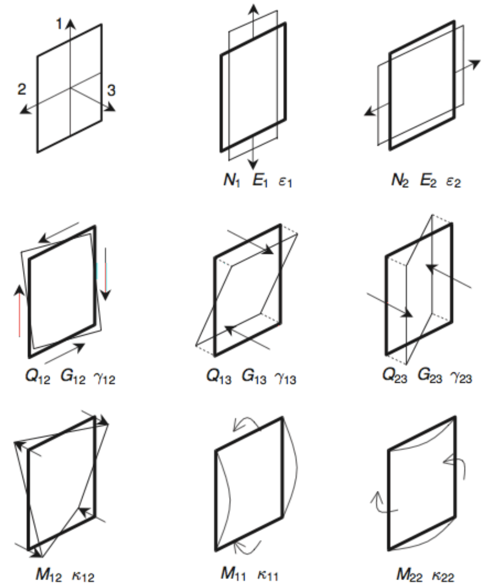

Figure 6. Definition of positive normal forces (N), shear forces (Q), and bending moments (M) for the CSP plate based on a local system of axes (Plaxis, 2013).

The flexural rigidity (EI) and axial stiffness (EA) of a corrugated pipe have different values depending on whether the cross section of interest is taken parallel or perpendicular to the corrugations. In reality, this is due to the significantly different geometrical properties (moment of inertia, I, and area, A) of the cross-sections in either direction, while the material properties (i.e. elastic modulus) are isotropic. However, since the cross-section of a plate element is rectangular in both directions, equivalent values of elastic modulus are assigned to the plate in the longitudinal (local axis-1) and circumferential (local axis-2) directions, such that (E'I') = (EI) and (E'A') = (EA). The material properties for the CSP plate used in the model are given in table 2. The effect of corrosion is a reduction in plate thickness. This change is reflected by reduced effective stiffness parameters, while the effective thickness remains unchanged. The effective unit weight of the plate, γ', must therefore be reduced so that the total weight, W, of the CSP reflects this loss of material (W = γ't').

Table 2. Material properties used for the CSP plate.

Equivalent Parameter	Intact (t =4.5 mm)	50% remaining (t = 2.25 mm)	25% remaining (t = 1.13 mm)
Thickness, t' (m)	0.0134	0.0134	0.0134
Elastic modulus (longitudinal), E'_1 (MPa)	7,574	6,380	118
Elastic modulus (circumferential), E'_2 (MPa)	72,400	67,915	17,050
Shear modulus, $G'_{12,13}$ (MPa)	19,690	18,596	4,923
Shear modulus, G'_{23} (MPa)	4,030	3,395	63
Cross-sectional area, A' (m^2/m)	0.0134	0.0134	0.0134
Moment of inertia, I' (m^4/m)	2.406E-6	3.008E-7	3.759E-8
Unit weight, γ' (kN/m^3)	27.8	13.9	6.950

Table 3. Material properties used for backfill soil and transitory soils.

Parameter	Backfill Soil (95% SPD)	Transitory Soil 1 (Compression Phase)	Transitory Soil 2 (Relaxation Phase)
Material Model	Mohr-Coulomb	Elastic	Elastic
Effective unit weight, γ' (kN/m^3)	21.9	21.9	21.9
Effective elastic modulus, E' (MPa)	60	6,000	60
Effective Poisson's ratio, v' (kPa)	0.3	0	0
Effective cohesion, c' (kPa)	2	N/A	N/A
Effective friction angle, φ' (°)	36	N/A	N/A

4.3 Soil/Interface Properties

The material properties used for the backfill soil and the transitory soils (see section 4.4.2) are summarized in Table 3. The backfill soil was modelled using an elasto-plastic stress-strain relationship (Mohr-Coulomb) in an attempt to capture the non-linear response of the culvert. No other soil models were used during the present study in order to minimize the model complexity. A small value (2 kPa) of effective cohesion, c', was assigned to the backfill soil for numerical stability. Interface properties between the soil and the CSP (soil/steel interface) were taken from the adjacent soil with a strength reduction factor, R_{inter} equal to 0.5.

4.4 Construction Sequence

4.4.1 Staged Construction

The backfill soil was activated in several phases using the staged construction mode in Plaxis 3D. In total, 12 layers with thicknesses of approximately 0.3 m (except for the 0.1 m-thick bedding layer directly beneath the pipe) were used as was done in the experimental test. However, each layer was applied in 3 phases for the reasons described in the following section, producing a total of 36 phases up to the completion of the backfilling with 0.9 m cover.

4.4.2 Simulation of Compaction Effects

Explicit modelling of the compaction process would add enormous complexity to the finite element model and was beyond the scope of this paper. An attempt was made, however, to simulate the effects of compaction as described earlier (i.e. to produce high residual lateral stresses with an approximately uniform distribution after backfilling). In the version of Plaxis 3D used for this study, it was not possible to specify a value of K during subsequent construction phases (lateral stresses are determined on the basis of Poisson's ration). A new approach to incorporate the compaction-induced lateral pressures was therefore devised.

The procedure used to model the effect of backfill compaction (see Figure 7) is as follows. The placement of each layer of backfill consists of three phases: addition, compression, and relaxation. In the first phase, the new soil layer is activated in order to generate geostatic vertical and horizontal stresses. In the second phase, a uniform horizontal surface load (of magnitude $\Delta\sigma'_h = K_p * \gamma z_c$, where z_c is taken as the layer thickness) is applied to the side boundaries of the current backfill layer. During this phase, the side boundaries are temporary released from their rollers and allowed to move freely in all directions, while the CSP plate is fixed. The soil layer is assigned transitory material properties of an ideal elastic material that is very stiff and has a Poisson's ratio of zero, such that it retains the entire applied horizontal stress. In the third phase, the side boundaries are returned to their original conditions of being fixed in the lateral directions (but free to move in the vertical direction), and the CSP plate is allowed to move freely in all directions. At the same time, the stiffness of the soil layer is returned to its original value (but remains elastic with zero Poisson's ratio) so that it attempts to relax against the side boundaries. This procedure results in "locked-in" horizontal stresses that are known to exist in compacted soil. For the soil layers placed between the invert and the crown of the CSP, a portion of these stresses dissipate as a result of lateral contraction of the culvert, and causes the peaking effect described earlier.

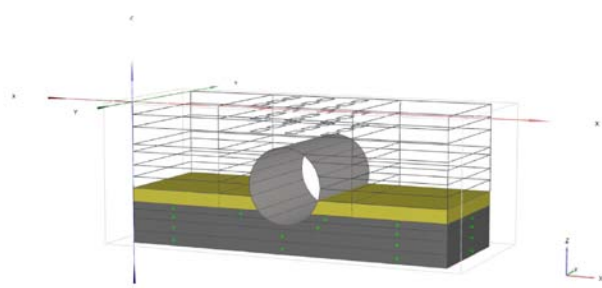

(a)

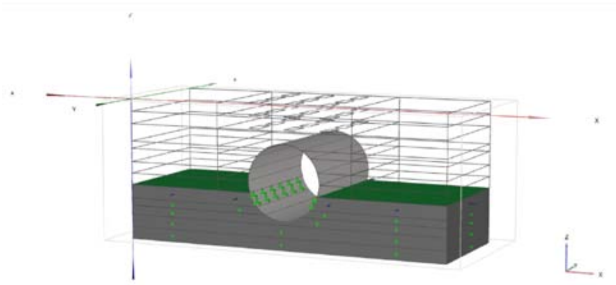

(b)

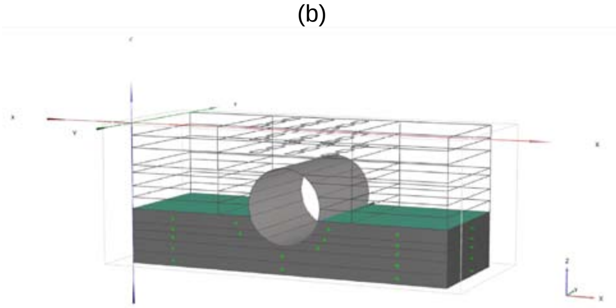

(c)

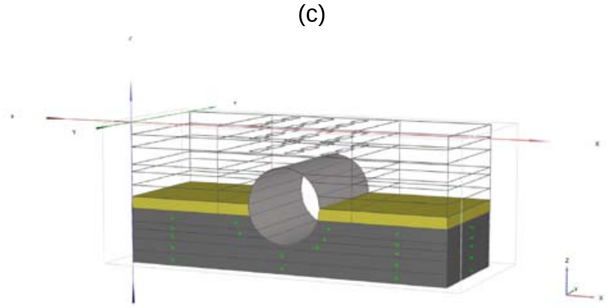

(d)

Figure 7. Procedure for simulating the effects of backfill compaction around a CSP culvert using transitory boundary conditions: (a) add layer ‘n’, (b) compress layer, (c) relax layer, and (d) add layer ‘n+1’

4.5 Loading

As mentioned earlier, the extension culverts (Figure 3) used in the experimental test were not included in the finite element model. Therefore, the loading scenarios used in the model were limited to those of a single wheel pair (SW), since the loaded areas of the single axle are within 0.5m of the model boundary and would introduce significant end effects. Live loads were applied to the intact culvert incrementally up to the CSA design load for cover heights of 0.9 m and 0.6 m.

4.6 Effects of Corrosion

An attempt was made to model the effects of corrosion (i.e. reduction in steel plate thickness) on the stability of the culvert. This was achieved by assigning reduced material properties to the CSP plate that reflect the reduction in pipe stiffness. Percentages of remaining plate thickness of 50% and 25% were considered, were applied across the entire bottom half of the pipe circumference (i.e. from 90° to 270° measured clockwise from the crown). The different load scenarios that were examined are listed in Table 4.

Table 4. Summary of loading scenarios (applied with cover heights of 0.9 m and 0.6 m).

Intact (t = 4.5 mm)	Bottom half corroded
06_SW_Intact	06_SW_50%_90_270[1]
	06_SW_25%_90_270
09_SW_Intact	09_SW_50%_90_270
	09_SW_25%_90_270[2]

[1] Denotes SW load with 0.6 m cover and CSP with thickness reduced to 50% around the bottom half of the pipe circumference.

[2] Denotes SA load with 0.9 m cover and CSP with thickness reduced to 25% around the bottom half of the pipe circumference.

5 MODEL RESULTS

5.1 Backfilling

5.1.1 Earth Pressure Distributions

The resulting vertical (σ'_{zz}) and horizontal (σ'_{xx}) effective stress distributions upon completion of backfilling with 0.9 m cover are shown in Figures 8 and 9, respectively. A value of K_p = 4 was used for determining the magnitude of the horizontal surface loads applied during the simulation of compaction effects. As can be seen, the distribution of vertical stresses is approximately linear from the ground surface to the bottom boundary. Meanwhile, the horizontal stress distribution is approximately uniform, with reductions in stress occurring immediately surrounding the pipe. It can also be seen that somewhat higher horizontal stresses occur below the pipe invert, where stress was not relieved due to contraction of the CSP. These distributions match closely with expected results for compacted backfill (as discussed in section 2).

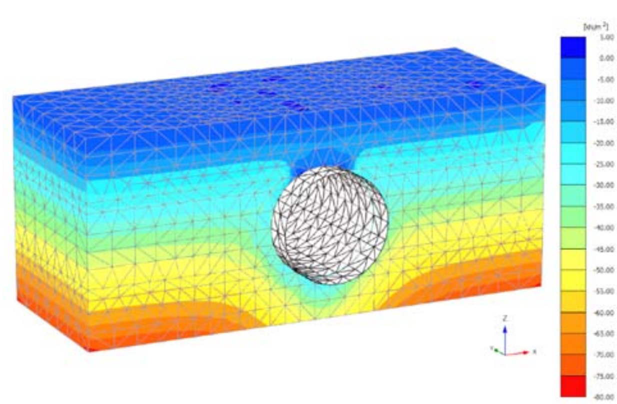

(a)

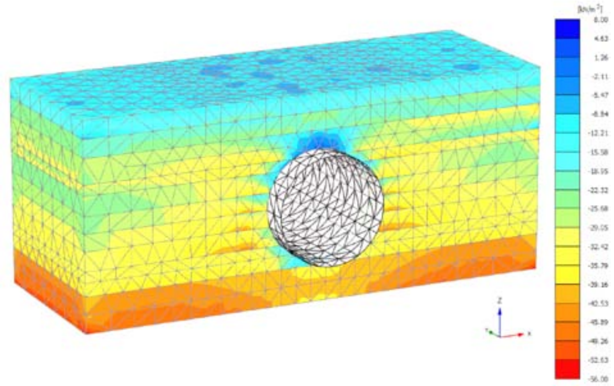

(b)

Figure 8. Distribution of (a) vertical effective stresses, σ'$_{zz}$ and (b) horizontal effective stresses, σ'$_{xx}$, upon completion of backfilling with 0.9 m cover.

5.1.2 Deflections

Figure 9 shows the change in both horizontal and vertical diameters for CSP2 during backfilling for the 3D finite element model (FEM) as well as the experimental results. All changes in vertical diameter were positive and all changes in horizontal diameter were negative, so the same data markers are used for deflection in either direction. One exception is the results of the 3D FEM when compaction effects were not simulated. In this case, vertical deflections were negative and horizontal deflections were positive and do not agree with the experimental results (i.e. peaking effect was not captured. The results of the 3D FEM match the experimental results quite closely when the effects of compaction are included. When the backfill reaches a height of 1.8 m above the invert (i.e. just reaches the crown), the CSP in the experiment responded with an increase of its vertical diameter by about 5.3 mm and a decrease of its horizontal diameter by about 6 mm, compared to 3D FEM results of 4.8 mm in either direction (i.e. within 10-20%). As the last 0.9 m of backfill (cover) is placed and compacted above the crown, vertical deflections from the model agree with the experimental results (contraction of about 1.5 mm), while the model slightly overestimates the horizontal deflection (expansion of 1.5 mm compared to 0.2 mm from experiment with 0.9 m cover). In general there appears to be a good correlation between the numerical and experimental results.

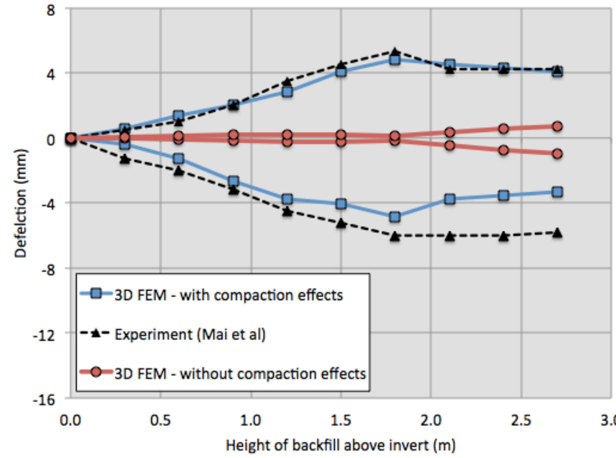

Figure 9. Pipe deflections during backfilling.

5.2 Live Loading

5.2.1 Deflections

The response of the culvert specimen in terms of change in vertical and horizontal diameter under live loading with 0.9 m cover is shown in Figure 10. It is evident that the FEM was able to capture the non-linear response of the culvert pipe, which would not have been possible if an elastic soil model was used. The calculated deflections from the 3D FEM at CSA design load (106 kN) are 0.7 and -2.2 mm in the horizontal and vertical directions, respectively. Measured deflections from the experimental test under the same loading conditions showed negligible change in the horizontal direction and a decrease of 2.0 mm in the vertical direction. The vertical deflection from the FEM is therefore in close agreement with the experimental results while the horizontal deflections are overestimated by the FEM. For both cover heights of 0.9 and 0.6 m, the 3D FEM provides a conservative estimate of deflection. However, the discrepancies between the model and the experimental results were larger when the cover height was reduced to 0.6 m (i.e. vertical contraction of 5 mm from the model compared to 2.5 mm from the experimental results under the CSA design load).

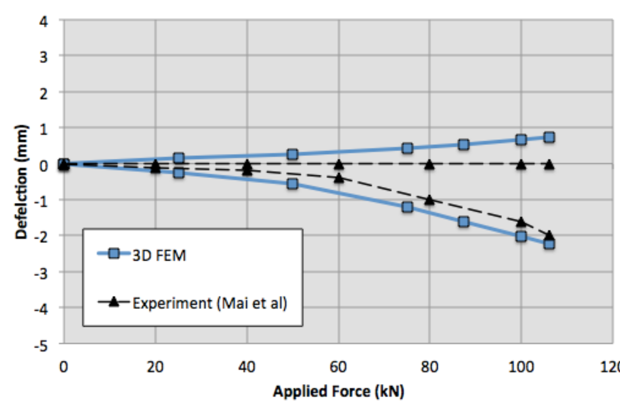

Figure 10. Pipe deflections during live loading with 0.9 m cover.

5.2.2 Thrusts

The maximum incremental thrusts in CSP2 from the numerical and experimental tests with 0.9m cover are plotted in Figure 11. Again it can be seen that the culvert is showing a non-linear response with increasing levels of live load. The predicted thrust forces in the culvert from the FEM at CSA design load were 30 and 46% greater than the experimental values for cover heights of 0.9 and 0.6 m, respectively.

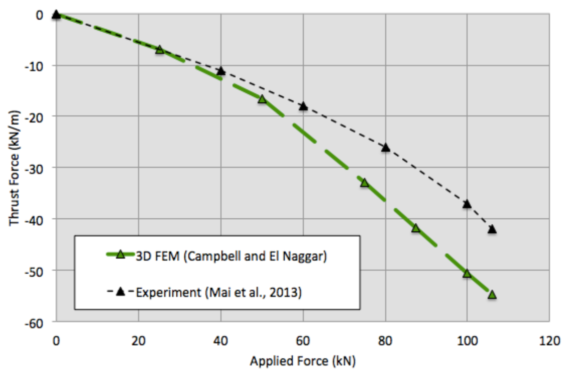

Figure 11. Maximum incremental thrust force under live load with 0.9 m cover

5.2.3 Bending Moments

Figure 12 presents the maximum incremental bending moments in CSP2 from the numerical and experimental tests. Once again there is a non-linear response of bending moment with increasing applied load, which was also observed in the experimental test. The FEM overestimated the bending moments for cover heights of 0.9 and 0.6 m, respectively when compared to experimental results.

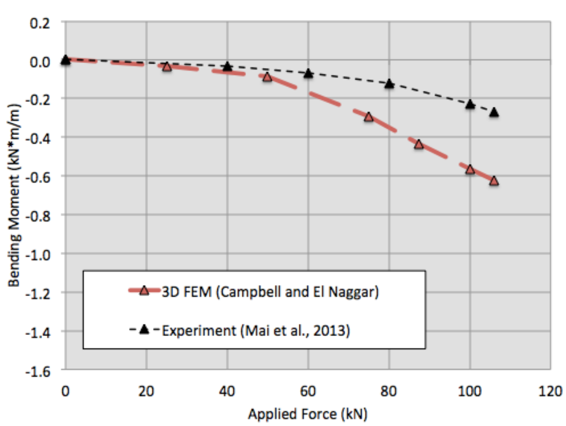

Figure 12. Maximum incremental bending moment under live load with 0.9 m cover

5.3 Effects of Reduced Plate Thickness

5.3.1 Deflections

Changes in vertical and horizontal deflections under live loading with 50% and 25% plate thickness remaining along the bottom half of the CSP were negligible when compared to the results with the CSP properties intact.

5.3.2 Thrusts

For the most part, thrust forces in the culvert did not change significantly when the plate thickness was reduced to 50% and 25%. However, a slight increase occurred just below the springline (where the material transitions from uncorroded to corroded). The increase can been clearly seen in Figure 13 (at locations 90 and 270 degrees from the crown) for a live load of 106kN and 0.9 m cover.

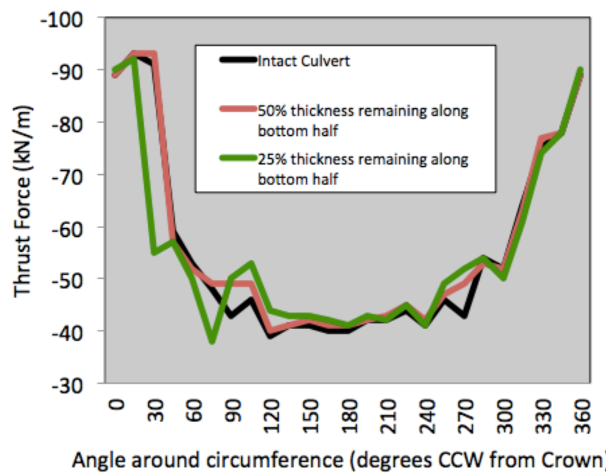

Figure 13. Localized thrust increase due to corrosion.

5.3.3 Moments

Negligible changes in bending moment distributions were observed when the CSP thickness was reduced to 50% and 25% along the bottom half, as compared to when intact CSP properties were used.

6 CONCLUSIONS

A detailed three-dimensional finite element model was developed to analyze the effects of corrosion on CSP culverts. The model included a new approach to incorporate the effects of soil compaction around the culvert. The results of the model upon completion of backfilling and after the application of live loads were compared to experimental test results. The following conclusions can be made based on the results of the current study:

- The approach used to simulate the effects of backfill soil compaction around the culvert resulted in a horizontal earth pressure distribution and culvert deflections that are more realistic than when compaction effects were not considered.

- The finite element model (FEM) was able to capture the peaking effect observed in the experimental tests during backfilling of CSP2. The changes in vertical diameter were within 10% of experimental values, while horizontal deflections were within 20%.
- The use of an elasto-plastic soil model allowed the non-linear response of the CSP culvert under live loading to be captured.
- Predicted deflections and thrust forces from the FEM were in reasonable agreement with experimental values
- Negligible changes in deflections and bending moments occur in the CSP when the thickness of the plate is reduced to 50% and 20% along the bottom half of the pipe.
- Minor changes thrust forces occur in the CSP when the thickness of the plate is reduced to 50% and 25% along the bottom half of the pipe. These increases take place just below the springline (where the transition from uncorroded to corroded material exists). However the reduced cross-sectional area of the culvert's wall due to the corrosion will cause a substantial increase in the stresses in the culvert.

REFERENCES

El-Sawy, K.M. 2003. Three-dimensional modeling of soil-steel culverts under the effects of truckloads, *Thin-Walled Structures*. 41: 747-768.

El-Taher, M. and Moore, I.D. 2008. Finite element study of stability of corroded metal culverts, *Transportation Research Record*, Journal of the Transportation Research Board. 2050: 157-166.

Ingold, T.S. 1979. The effects of compaction on retaining walls, *Geotechnique*, 29(3): 265-283.

MacDonald, L. 2010. Numerical modeling of buried orthotropic steel shell structures, Master thesis, Dalhousie University, Halifax, Nova Scotia, Canada.

Mai, V., Hoult, N., and Moore, I. 2014. Effect of Deterioration on the Performance of Corrugated Steel Culverts, *J. Geotech. Geoenviron. Eng.*, 140(2), 04013007.

Mai, V., Moore, I., and Hoult, N. 2014. Performance of two-dimensional analysis: Deteriorated metal culverts under surface live load, *Tunelling and Underground Space Technology,* 42: 152-160

Mai, V.T. 2013 Assessment of deteriorated corrugated steel culverts, *Master thesis*, Queen's University, Kingston, Ontario, Canada.

Moore, I.D., and Taleb, B. 1999. Metal culvert response to live loading: Performance of three-dimensional analysis. *Transportation Research Record*, Journal of the Transportation Research Board. 1656: 37-44.

Perrin, J. and Jhaveri, C.S. 2004. The economic costs of culvert failures, *TRB 2004 Annual Meeting CD-ROM*, Transportation Research Board, Washington, DC, USA.

Plaxis, 2012. *Plaxis Standard Course*, Course Notes, Delft University of Technology, Mumbai, India.

Plaxis, 2013. *Plaxis 3D Reference Manual*.

USACE. 1998. Engineering and design conduits, culverts and pipes, *Engineer Manual 1110-2-2902*, U.S. Army Corps of Engineer, Washington, D.C.

Watkins, R.K. and Anderson, L.R. 2000. *Structural Mechanics of Buried Pipes*, CRC Press, Boca Raton, Florida, USA.